Preliminary aeroelastic design of composite wings with distributed electric propulsion

Wang, Zhijun; Liu Xu, Vanessa Q.; De Breuker, Roeland

Publication date
2022

Published in
Proceedings of the International Forum of Aeroelasticity and Structural Dynamics 2022, IFASD 2022

Citation (APA)
Wang, Z., Liu Xu, V. Q., & De Breuker, R. (2022). Preliminary aeroelastic design of composite wings with distributed electric propulsion. In P. Fajardo (Ed.), *Proceedings of the International Forum of Aeroelasticity and Structural Dynamics 2022, IFASD 2022* (Proceedings of the International Forum of Aeroelasticity and Structural Dynamics 2022, IFASD 2022). International Forum on Aeroelasticity and Structural Dynamics (IFASD).

Important note
To cite this publication, please use the final published version (if applicable).
Please check the document version above.

International Forum on Aeroelasticity and Structural Dynamics
IFASD 2022
13-17 June 2022, Madrid, Spain

PRELIMINARY AEROELASTIC DESIGN OF COMPOSITE WINGS WITH DISTRIBUTED ELECTRIC PROPULSION

Zhijun Wang[1], **Vanessa Q. Liu Xu**[1], **Roeland De Breuker**[1]

[1]Faculty of Aerospace Engineering
Delft University of Technology
Kluyverweg 1, 2629 HS Delft, The Netherlands
Z.Wang-16@tudelft.nl

Keywords: Aeroelastic optimization, whirl flutter, composite wings, electric aircraft, DEP

Abstract: In the development of electric aircraft, the use of distributed electric propulsion introduces a potential occurrence of propeller whirl flutter, which needs to be taken into account for wing structural design. To this end, this work extends an in-house aeroelastic optimization tool by means of including a post-processing procedure on whirl flutter analysis. In aeroelastic optimization, propellers are modeled as concentrated masses, and the wing mass is minimized by tailoring the lamination parameters and thickness of wing laminates subject to aerostructural design constraints. For the whirl flutter analysis of the optimized wing, a new aeroelastic model is built by coupling propeller motions and aerodynamic loads into wing aeroelastic model. The usefulness of the purposed approach is demonstrated using a numerical example, where the required inputs on propeller mounting properties are determined via a parametric study. The result indicates that flexibly mounting propellers on a flexible wing leads to the decrease of wing flutter speed, and it also confirms that the propeller mounting properties have a large influence on aeroelastic instability of the coupled propeller-wing system.

1 INTRODUCTION

Driving by the goal of reducing in-flight emissions in civil aviation, the concept of hybrid/all-electric aircraft has drawn a lot of attention in recent years [1]. In comparison to the conventional aircraft powered by gas turbine engines, the required lift and thrust of electric aircraft are generated using multiple propellers spread across the wing span, which, usually is referred to as Distributed Electric Propulsion (DEP). Currently, due to the limitation of battery technologies, DEP aircraft usually are equipped with high aspect ratio wings for increasing the aerodynamic efficiency and reducing the weight of aircraft [2].

It is well known that a thinner wing with high aspect ratio tends to be more flexible and therefore undergoes large deformations, which makes the aeroelastic instabilities, e.g. wing flutter, become more critical for wing design. Further, since the propellers are flexibly mounted on the wing, another dynamic instability phenomena, propeller whirl flutter, may occur in the operation of electric aircraft. In principle, whirl flutter is attributed to the additional forces and moments induced by the propeller aerodynamics, which drives the airframe/pylon motions to become unstable due to gyroscopic effects [3]. The occurrence of classical wing flutter and/or propeller whirl flutter can cause severe damage on aircraft structures and even lead to fatal accidents. Therefore, it is of great importance to take these aeroelastic instabilities into account in the preliminary design of DEP aircraft wings.

Despite the aeroelastic stability has been widely studied in the design of conventional (high aspect ratio) aircraft wings [4], the methods and findings of those studies may not be directly applied to the design of DEP aircraft wings, because the presence of the propellers have a large impact on aerodynamic and structural characteristics of the wing [5]. On the one hand, rotating propellers add extra mass and inertia to wing structure, and, from the aerodynamic perspective, they help the wing generate lift via blowing the air around the wing [6]. On the other hand, wing deformation leads to the change of propeller position, which affects propeller aerodynamics and, in return, results in different wing deformations.

In order to account for the effect of propellers on wing aeroelastic characteristics, Amoozgar et al. [5] model the electric propeller as a concentrated mass attached to the wing and include the propeller thrust force as a follower force for constructing aeroelastic governing equations. Hoover et al. [3, 7] together with Heeg et al. [8] have carried out several studies on propeller whirl flutter stability for the development of the NASA X-57 electric aircraft. In their work, the widely used multibody dynamics simulation tools [9, 10] developed for turboprop and tilt rotor aircraft [11–13] are employed. Recently, Böhnisch et al. [14] proposed an aeroelastic model to analyze whirl flutter of DEP wings, in which the propeller is connected to a flexible wing via a rigid pylon with pitch and yaw motions. Additionally, the propeller pylon also can be modeled using beam elements [15] in order to improve the fidelity of propeller structural model.

Currently, there is a limited number of studies on whirl flutter of DEP wings according to the literature survey. Furthermore, to the best of authors' knowledge, almost all existing researches focus on whirl flutter analysis of the given wing designs. While the field of wing sizing for DEP aircraft with the consideration of propeller whirl flutter seems to be unexplored. Accordingly, the main objective of this work is to develop a new functionality of whirl flutter analysis for an in-house optimization tool named PROTEUS [16]. Such that the extended version of PROTEUS is capable to aeroelastically tailor the wing laminates of DEP aircraft for minimal wing mass with the maintenance of the whirl flutter stability margins.

Further, the extended PROTEUS is used to design the wing structure of a hybrid-electric aircraft in GENESIS (Gauging the ENvironmEntal Sustainability of electrIc aircraft Systems) project. GENESIS project is funded by the Clean Sky 2 Joint Undertaking, and it aims to develop a technology and sustainability roadmap to support the ambitions of the European aviation industry for transitioning towards environmentally sustainable and competitive electric and hybrid aircraft systems. The present work is carried out within work package 1: Basic Concepts & Requirement Analysis, where the reference DEP configuration and the related aircraft data are provided by University of Naples Federico II (UNINA), one of project partners in GENESIS.

2 METHODOLOGY

In the present work, the design procedure proposed for DEP wings includes two steps: 1) aeroelastic tailoring through optimizing composite wing structures without considering whirl flutter effect; 2) whirl flutter analysis for assessing the feasibility of the optimized wing. Aeroelastic optimization is carried out using PROTEUS, and the related methods are reviewed in Section 2.1. For whirl flutter assessment, an aeroelastic model of the coupled propeller-wing system is built within the framework of PROTEUS in Section 2.2.

2.1 Aeroelastic optimization

For the design of composite wing structures, an in-house tool named PROTEUS [16], is used to tailor the stiffness properties of wing laminates, so that the wing mass can be minimized subject

to aerostructural design constraints. Within the framework of PROTEUS, wing skins and spars are partitioned into a series of design sections, of which the independent lamination parameters and thickness assigned to each section are defined as design variables.

For aeroelastic analysis, the load carrying structure, i.e., wing-box, is modeled as a clamped beam using a geometrically nonlinear beam Finite Element Model (FEM). Accordingly, the wing structural response can be approximated by solving the following dynamic structural model:

$$\boldsymbol{M}_{\mathrm{w}}\ddot{\boldsymbol{q}}_{\mathrm{w}} + \boldsymbol{K}_{\mathrm{w}}\boldsymbol{q}_{\mathrm{w}} = \boldsymbol{Q}_{\mathrm{w}}\,, \tag{1}$$

where $\boldsymbol{q}_{\mathrm{w}}$ contains wing structural degrees of freedom (DOF), $\boldsymbol{M}_{\mathrm{w}}$ and $\boldsymbol{K}_{\mathrm{w}}$ are the global mass and stiffness matrices, respectively. $\boldsymbol{Q}_{\mathrm{w}}$ is the equivalent nodal forces and moments derived from wing aerodynamic forces and moments through

$$\boldsymbol{Q}_{\mathrm{w}} = \boldsymbol{T}_{\mathrm{AS}}\boldsymbol{R}_{\alpha}\boldsymbol{Q}^{\mathrm{a}}_{\mathrm{w}}\,, \tag{2}$$

where $\boldsymbol{T}_{\mathrm{AS}}$ is a transformation matrix from wing aerodynamic to structural forces, $\boldsymbol{R}_{\alpha}$ is a coordinate transformation matrix used to rotate the wing aerodynamic forces through the aircraft angle of attack, α, to the body-fixed coordinate system. $\boldsymbol{Q}^{\mathrm{a}}_{\mathrm{w}}$ contains the aerodynamic forces and moments obtained from wing aerodynamic analysis. In PROTEUS, the wing aerodynamic response is predicted using lattice vortex method based on potential flow theory. Accordingly, the wing aerodynamic forces and moments can be obtained by

$$\boldsymbol{Q}^{\mathrm{a}}_{\mathrm{w}} = \boldsymbol{H}_3\boldsymbol{T}_1\boldsymbol{x}_{\mathrm{w}} + \boldsymbol{H}_4\boldsymbol{T}_2\dot{\boldsymbol{x}}_{\mathrm{s}} + \boldsymbol{L}_3\boldsymbol{B}_{\alpha}\dot{\boldsymbol{\alpha}}_{\mathrm{air}}\,, \tag{3}$$

where $\boldsymbol{x}_{\mathrm{s}} = [\dot{\boldsymbol{q}}^{\mathrm{T}}_{\mathrm{w}}, \boldsymbol{q}^{\mathrm{T}}_{\mathrm{w}}]^{\mathrm{T}}$ is the wing structural state vector, and $\boldsymbol{x}_{\mathrm{w}}$ represents the aeroelastic state vector of the flexible wing. Defining $\boldsymbol{x}_{\mathrm{a}} = [\boldsymbol{\Gamma}^{\mathrm{T}}_{\mathrm{w}}, \boldsymbol{\alpha}^{\mathrm{T}}_{\mathrm{air}}]^{\mathrm{T}}$ as the wing aerodynamic state vector, where $\boldsymbol{\Gamma}_{\mathrm{w}}$ are the vortex strengths of the aerodynamic panels in aerodynamic analysis model, and $\boldsymbol{\alpha}_{\mathrm{air}}$ refers to the perturbation angles of attack of the aerodynamic panels induced by the free stream flow. Then the aeroelastic state vector can be expressed as $\boldsymbol{x}_{\mathrm{w}} = [\boldsymbol{x}^{\mathrm{T}}_{\mathrm{a}}, \boldsymbol{x}^{\mathrm{T}}_{\mathrm{s}}]^{\mathrm{T}}$, and the following relationship holds:

$$\dot{\boldsymbol{x}}_{\mathrm{a}} = \boldsymbol{H}_1\boldsymbol{T}_1\boldsymbol{x}_{\mathrm{w}} + \boldsymbol{H}_2\dot{\boldsymbol{\alpha}}_{\mathrm{air}}\,. \tag{4}$$

Note that the calculation of matrices $\boldsymbol{H}_1$, $\boldsymbol{H}_2$ $\boldsymbol{H}_3$, $\boldsymbol{H}_4$, $\boldsymbol{T}_1$, $\boldsymbol{T}_2$, $\boldsymbol{L}_3$ and $\boldsymbol{B}_{\alpha}$ in equations (3) and (4) can be found in [16].

In PROTEUS, wing ribs and the wing associated structures, such as control surfaces, fuel tanks and propellers, are modeled as concentrated masses, as an example depicted in Figure 1. In this way, the effect of the distributed electric propellers on wing sizing can be considered by including the mass inertia into the global mass matrix $\boldsymbol{M}_{\mathrm{w}}$ in equation (1).

In the present work, the optimization constraints considered for wing sizing cover wing aeroelastic stability, local angle of attack, aileron effectiveness, material strength, buckling load and

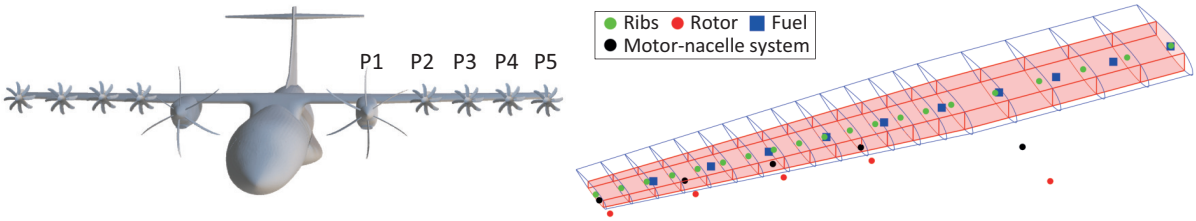

(a) A regional DEP aircraft **(b)** Wing structural analysis model

Figure 1: Illustration of (a) a regional DEP aircraft (provided by GENESIS partner UNINA) and its (b) wing structural analysis model generated using an in-house tool named PROTEUS.

lamination feasibility. The aeroelastic stability is implemented by restricting the real part of the eigenvalues in the dynamic aeroelastic state-space system. The local angle of attack at each aerodynamic cross-section is restricted in order to ensure attached aerodynamic flow. Further, a minimum aileron effectiveness has to be achieved for ensuring the aileron performance. For the measurement of composite strength, the Tsai-Wu failure criterion derived in terms of lamination parameters and principal strains [17, 18] is employed. The critical buckling load is governed by the inverse buckling factor measured at each wing skin panel delimited by the ribs and stiffeners [19]. Additionally, the lamination feasibility formulations [20–22] are applied to ensure the lamination parameters represent a feasible laminate. For further details on PROTEUS, one may refer to the work presented in [16, 23].

2.2 Whirl flutter analysis

Originally, PROTEUS is developed for the aeroelastic tailoring of conventional wing structures, and it lacks the capability to take propeller whirl flutter into account for wing sizing. To overcome this limitation, in this section, a new functionality of whirl flutter analysis is developed for PROTEUS on the basis of authors' previous work presented in [24]. This functionality is incorporated into PROTEUS as a post-processing procedure, which aims to assess the whirl flutter of the optimized DEP wing.

For a flexible wing with a flexibly mounted propeller, as illustrated in Figure 2, the propeller motion can be described using 2 DOF: Pitch θ and yaw ψ angles. Accordingly, DEP wing can be modeled as a propeller-pylon-wing system, in which the propeller attached to a rigid pylon and mounted on the wing with given pitch $\boldsymbol{K}_\theta$ and yaw $\boldsymbol{K}_\psi$ stiffnesses assigned to pitch and yaw pivot points, respectively. The positions of pivot points vary with the wing deformation described by the (vertical) displacement h and twist α of beam nodes. This means that, from the implementation point of view, the propellers need to be connected to beam nodes in the present propeller-pylon-wing model.

It is important to note that, the propellers studied in this work have fixed-pitch blades and they are in windmilling conditions. Accordingly, the propeller advance ratio is constant, which can be determined according to the given geometric collective pitch angle. The propeller rotational speed varies with the airspeed to maintain the advance ratio. In addition, the propeller structure is lumped into two concentrated masses: 1) Rotor mass, illustrated as a red dot in Figure 1(b), representing the spinner and blades, 2) motor-nacelle system mass, a black dot in Figure 1(b), describing the motor, nacelle and other system components.

The equations of motion of the aforementioned propeller-pylon-wing system can be derived using Lagrange's equations, refer to authors' previous work [24]. Note that the wing structure is modeled based on typical section theory in [24], which requires the location of wing elastic

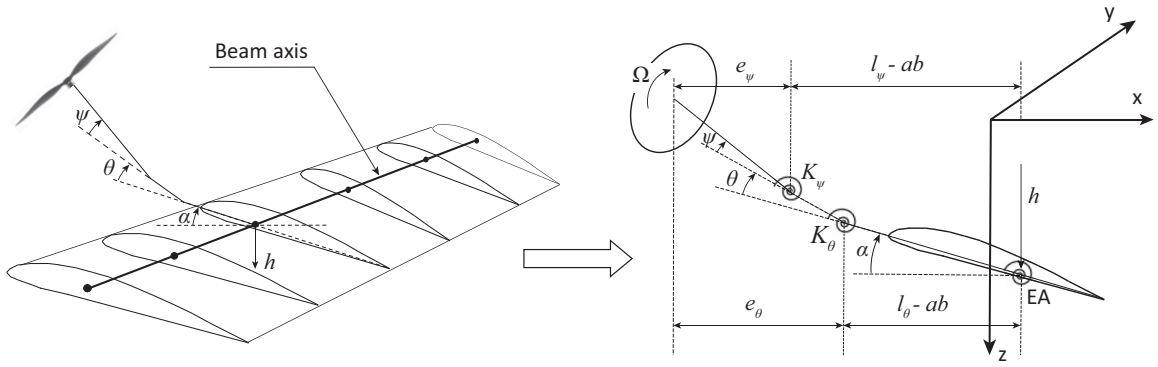

Figure 2: Illustration of a propeller-pylon-wing model with the main parameters indicated for the derivation of equations of motion and propeller aerodynamics [24].

axis, as indicated as EA in Figure 2. However, this is not the case for the wing structural model implemented in PROTEUS as introduced in Section 2.1. Nevertheless, as the wing deformation is described in terms of beam reference axis, the derivations presented in [24] still hold when the elastic axis is defined as beam reference axis. As a result, the non-dimensional distance a indicated in Figure 2 refers to the distance between beam reference axis and mid-point of airfoil chord non-dimensionalized with respect to the semi-chord b. As given in [24], the structural dynamic model of a flexibly mounted propeller can be formulated as

$$\boldsymbol{A}_\mathrm{s}\ddot{\boldsymbol{q}}_\mathrm{p} + \boldsymbol{B}_\mathrm{s}\ddot{\boldsymbol{q}}_\mathrm{wp} + \boldsymbol{C}_\mathrm{s}\dot{\boldsymbol{q}}_\mathrm{p} + \boldsymbol{D}_\mathrm{s}\dot{\boldsymbol{q}}_\mathrm{wp} + \boldsymbol{E}_\mathrm{s}\boldsymbol{q}_\mathrm{p} = \boldsymbol{Q}_\mathrm{p}\,, \tag{5}$$

where $\boldsymbol{q}_\mathrm{p} = [\theta, \psi]^\mathrm{T}$ are the generalized coordinates of propeller, $\boldsymbol{q}_\mathrm{wp} = [h, \alpha]^\mathrm{T}$ are the wing nodal displacement and twist at the section where the propeller is placed, and $\boldsymbol{Q}_\mathrm{p}$ refers to propeller aerodynamic loads. The calculation of the structural mass matrices $\boldsymbol{A}_\mathrm{s}$ and $\boldsymbol{B}_\mathrm{s}$, the structural damping matrices $\boldsymbol{C}_\mathrm{s}$ and $\boldsymbol{D}_\mathrm{s}$, and the structural stiffness matrix $\boldsymbol{E}_\mathrm{s}$ can be found in [24].

The propeller aerodynamics is calculated using Houbolt-Reed's method [25], which employs 16 aerodynamic derivatives to express the aerodynamic loads acting on a rotating propeller. As a result, the propeller aerodynamic forces and moments $\boldsymbol{Q}_\mathrm{p}$ can be formulated as

$$\boldsymbol{Q}_\mathrm{p} = \boldsymbol{A}_\mathrm{a}\ddot{\boldsymbol{q}}_\mathrm{p} + \boldsymbol{B}_\mathrm{a}\ddot{\boldsymbol{q}}_\mathrm{wp} + \boldsymbol{C}_\mathrm{a}\dot{\boldsymbol{q}}_\mathrm{p} + \boldsymbol{D}_\mathrm{a}\dot{\boldsymbol{q}}_\mathrm{wp} + \boldsymbol{E}_\mathrm{a}\boldsymbol{q}_\mathrm{p} + \boldsymbol{F}_\mathrm{a}\boldsymbol{q}_\mathrm{wp}\,, \tag{6}$$

where the aerodynamic mass matrices $\boldsymbol{A}_\mathrm{a}$ and $\boldsymbol{B}_\mathrm{a}$, the aerodynamic damping matrices $\boldsymbol{C}_\mathrm{a}$ and $\boldsymbol{D}_\mathrm{a}$, and the aerodynamic stiffness matrices $\boldsymbol{E}_\mathrm{a}$ and $\boldsymbol{F}_\mathrm{a}$ are provided in [24].

Combining equations (5) and (6), and substituting the vector $\boldsymbol{q}_\mathrm{wp}$ by wing generalized coordinates $\boldsymbol{q}_\mathrm{w}$, the aeroelastic model for a flexibly mounted propeller is

$$(\boldsymbol{A}_\mathrm{s} - \boldsymbol{A}_\mathrm{a})\,\ddot{\boldsymbol{q}}_\mathrm{p} + (\boldsymbol{B}_\mathrm{sg} - \boldsymbol{B}_\mathrm{ag})\,\ddot{\boldsymbol{q}}_\mathrm{w} + (\boldsymbol{C}_\mathrm{s} - \boldsymbol{C}_\mathrm{a})\,\dot{\boldsymbol{q}}_\mathrm{p} + (\boldsymbol{D}_\mathrm{sg} - \boldsymbol{D}_\mathrm{ag})\,\dot{\boldsymbol{q}}_\mathrm{w} + (\boldsymbol{E}_\mathrm{s} - \boldsymbol{E}_\mathrm{a})\,\boldsymbol{q}_\mathrm{p} - \boldsymbol{F}_\mathrm{ag}\boldsymbol{q}_\mathrm{w} = \boldsymbol{0}\,, \tag{7}$$

where $\boldsymbol{B}_\mathrm{sg}$, $\boldsymbol{B}_\mathrm{ag}$, $\boldsymbol{D}_\mathrm{sg}$, $\boldsymbol{D}_\mathrm{ag}$ and $\boldsymbol{F}_\mathrm{ag}$ refer to the global form of $\boldsymbol{B}_\mathrm{s}$, $\boldsymbol{B}_\mathrm{a}$, $\boldsymbol{D}_\mathrm{s}$, $\boldsymbol{D}_\mathrm{a}$ and $\boldsymbol{F}_\mathrm{a}$, respectively. These global matrices are obtained by restructuring their counterparts according to the location of the beam node attached to propeller.

For a wing with DEP units, the inclusion of rotating propellers adds extra mass and inertial terms into the wing structural model due to propeller mass and gyroscopic effect. Further, to account for the propeller aerodynamic effect on the wing, the propeller aerodynamic loads are added as nodal forces and moments acting on wing structural model. According to the equations of motion of the propeller-pylon-wing system [24] and the wing structural dynamic model (1), the dynamic structural model of a propeller-pylon-wing system can be formulated as

$$\boldsymbol{M}_{\mathrm{w}}\ddot{\boldsymbol{q}}_{\mathrm{w}} + \boldsymbol{K}_{\mathrm{w}}\boldsymbol{q}_{\mathrm{w}} + \boldsymbol{F}_{\mathrm{sg}}\ddot{\boldsymbol{q}}_{\mathrm{p}} + \boldsymbol{G}_{\mathrm{sg}}\ddot{\boldsymbol{q}}_{\mathrm{w}} + \boldsymbol{H}_{\mathrm{sg}}\dot{\boldsymbol{q}}_{\mathrm{p}} = \boldsymbol{Q}_{\mathrm{w}} + \boldsymbol{Q}_{\mathrm{pw}}\,, \tag{8}$$

where $\boldsymbol{F}_{\mathrm{sg}}$, $\boldsymbol{G}_{\mathrm{sg}}$ and $\boldsymbol{H}_{\mathrm{sg}}$ are the propeller mass and inertial terms added on the wing structural model. Similarly, they are also restructured into global form according to propeller position, and one may refer to [24] for more details. It is important to note that, in the above equation, the global mass $\boldsymbol{M}_{\mathrm{w}}$ and stiffness $\boldsymbol{K}_{\mathrm{w}}$ matrices of the wing are obtained from PROTEUS without adding propeller concentrated masses. Further, $\boldsymbol{Q}_{\mathrm{pw}}$ are the propeller aerodynamic loads acting on wing (vertical) displacement h and twist α, which are

$$\boldsymbol{Q}_{\mathrm{pw}} = \boldsymbol{P}_{1\mathrm{g}}\ddot{\boldsymbol{q}}_{\mathrm{p}} + \boldsymbol{P}_{2\mathrm{g}}\ddot{\boldsymbol{q}}_{\mathrm{w}} + \boldsymbol{P}_{3\mathrm{g}}\dot{\boldsymbol{q}}_{\mathrm{p}} + \boldsymbol{P}_{4\mathrm{g}}\dot{\boldsymbol{q}}_{\mathrm{w}} + \boldsymbol{P}_{5\mathrm{g}}\boldsymbol{q}_{\mathrm{p}} + \boldsymbol{P}_{6\mathrm{g}}\boldsymbol{q}_{\mathrm{w}}\,, \tag{9}$$

where $\boldsymbol{P}_{1\mathrm{g}}$ to $\boldsymbol{P}_{6\mathrm{g}}$ can be found in [24], note that they are also the restructured global form because the vector $\boldsymbol{q}_{\mathrm{wp}}$ is replaced by $\boldsymbol{q}_{\mathrm{w}}$.

Defining vector $\boldsymbol{q} = [\boldsymbol{q}_{\mathrm{w}}^{\mathrm{T}}, \boldsymbol{q}_{\mathrm{p}}^{\mathrm{T}}]^{\mathrm{T}}$ to represent the DOF of the propeller-pylon-wing system, and combining equations (7) - (9) and (2), then the dynamic structural model of the wing including propeller effects (from both aerodynamic and structural aspects) can be formulated as

$$\boldsymbol{M}_{\mathrm{wp}}\ddot{\boldsymbol{q}} + \boldsymbol{C}_{\mathrm{wp}}\dot{\boldsymbol{q}} + \boldsymbol{K}_{\mathrm{wp}}\boldsymbol{q} = \boldsymbol{\Phi}_1\boldsymbol{T}_{\mathrm{AS}}\boldsymbol{R}_{\alpha}\boldsymbol{Q}_{\mathrm{w}}^{\mathrm{a}}\,, \tag{10}$$

with

$$\boldsymbol{M}_{\mathrm{wp}} = \begin{bmatrix} \boldsymbol{M}_{\mathrm{w}} + \boldsymbol{G}_{\mathrm{sg}} - \boldsymbol{P}_{2\mathrm{g}} & \boldsymbol{F}_{\mathrm{sg}} - \boldsymbol{P}_{1\mathrm{g}} \\ \boldsymbol{B}_{\mathrm{sg}} - \boldsymbol{B}_{\mathrm{ag}} & \boldsymbol{A}_{\mathrm{s}} - \boldsymbol{A}_{\mathrm{a}} \end{bmatrix}, \quad \boldsymbol{C}_{\mathrm{wp}} = \begin{bmatrix} -\boldsymbol{P}_{4\mathrm{g}} & \boldsymbol{H}_{\mathrm{sg}} - \boldsymbol{P}_{3\mathrm{g}} \\ \boldsymbol{D}_{\mathrm{sg}} - \boldsymbol{D}_{\mathrm{ag}} & \boldsymbol{C}_{\mathrm{s}} - \boldsymbol{C}_{\mathrm{a}} \end{bmatrix},$$
$$\boldsymbol{K}_{\mathrm{wp}} = \begin{bmatrix} \boldsymbol{K}_{\mathrm{w}} - \boldsymbol{P}_{6\mathrm{g}} & -\boldsymbol{P}_{5\mathrm{g}} \\ -\boldsymbol{F}_{\mathrm{ag}} & \boldsymbol{E}_{\mathrm{s}} - \boldsymbol{E}_{\mathrm{a}} \end{bmatrix}, \tag{11}$$

and $\boldsymbol{\Phi}_1 = [\boldsymbol{I}, \boldsymbol{0}]^{\mathrm{T}}$. Accordingly, by defining $\boldsymbol{x}_{\mathrm{wp}} = \left[\dot{\boldsymbol{q}}^{\mathrm{T}}, \boldsymbol{q}^{\mathrm{T}}\right]^{\mathrm{T}}$, the structural state-space system can be expressed as

$$\dot{\boldsymbol{x}}_{\mathrm{wp}} = \boldsymbol{A}_{\mathrm{wp}}\boldsymbol{x}_{\mathrm{wp}} + \boldsymbol{B}_{\mathrm{wp}}\boldsymbol{\Phi}_1\boldsymbol{T}_{\mathrm{AS}}\boldsymbol{R}_{\alpha}\boldsymbol{Q}_{\mathrm{w}}^{\mathrm{a}}\,, \tag{12}$$

where

$$\boldsymbol{A}_{\text{wp}} = \begin{bmatrix} -\boldsymbol{M}_{\text{wp}}^{-1}\boldsymbol{C}_{\text{wp}} & -\boldsymbol{M}_{\text{wp}}^{-1}\boldsymbol{K}_{\text{wp}} \\ \boldsymbol{I} & \boldsymbol{0} \end{bmatrix}, \quad \boldsymbol{B}_{\text{wp}} = \begin{bmatrix} \boldsymbol{M}_{\text{wp}}^{-1} \\ \\ \boldsymbol{0} \end{bmatrix}. \tag{13}$$

Further, to insert equation (3) into equation (12), firstly, equation (3) is reformulated as

$$\boldsymbol{Q}_{\text{w}}^{\text{a}} = \boldsymbol{H}_3\boldsymbol{T}_1\boldsymbol{\Phi}_2\boldsymbol{x} + \boldsymbol{H}_4\boldsymbol{T}_2\boldsymbol{\Phi}_3\dot{\boldsymbol{x}}_{\text{wp}} + \boldsymbol{L}_3\boldsymbol{B}_\alpha\dot{\boldsymbol{\alpha}}_{\text{air}}\,, \tag{14}$$

where $\boldsymbol{x} = \left[\boldsymbol{\Gamma}_{\text{w}}^{\text{T}}, \boldsymbol{\alpha}_{\text{air}}^{\text{T}}, \dot{\boldsymbol{q}}_{\text{w}}^{\text{T}}, \dot{\boldsymbol{q}}_{\text{p}}^{\text{T}}, \boldsymbol{q}_{\text{w}}^{\text{T}}, \boldsymbol{q}_{\text{p}}^{\text{T}}\right]^{\text{T}}$ is the state vector for the propeller-pylon-wing system, $\boldsymbol{\Phi}_2$ and $\boldsymbol{\Phi}_3$ are matrices containing zeros and ones, which are used to select $\boldsymbol{x}_{\text{w}}$ from $\boldsymbol{x}$, $\dot{\boldsymbol{x}}_{\text{s}}$ from $\dot{\boldsymbol{x}}_{\text{wp}}$, respectively. Then, inserting (14) into (12), the aeroelastic model can be expressed as

$$\dot{\boldsymbol{x}}_{\text{wp}} = \boldsymbol{H}_5^{-1}\boldsymbol{H}_6\boldsymbol{x} + \boldsymbol{H}_5^{-1}\boldsymbol{H}_7\dot{\boldsymbol{\alpha}}_{\text{air}}\,, \tag{15}$$

with

$$\begin{aligned} &\boldsymbol{H}_5 = \boldsymbol{I} - \boldsymbol{B}_{\text{wp}}\boldsymbol{\Phi}_1\boldsymbol{T}_{\text{AS}}\boldsymbol{R}_\alpha\boldsymbol{H}_4\boldsymbol{T}_2\boldsymbol{\Phi}_3\,, \qquad \boldsymbol{H}_6 = \boldsymbol{A}_{\text{wp}}\boldsymbol{\Phi}_4 + \boldsymbol{B}_{\text{wp}}\boldsymbol{\Phi}_1\boldsymbol{T}_{\text{AS}}\boldsymbol{R}_\alpha\boldsymbol{H}_3\boldsymbol{T}_1\boldsymbol{\Phi}_2\,, \\ &\boldsymbol{H}_7 = \boldsymbol{B}_{\text{wp}}\boldsymbol{\Phi}_1\boldsymbol{T}_{\text{AS}}\boldsymbol{R}_\alpha\boldsymbol{L}_3\boldsymbol{B}_\alpha\,, \end{aligned} \tag{16}$$

where $\boldsymbol{\Phi}_4$ is used to select $\boldsymbol{x}_{\text{wp}}$ from $\boldsymbol{x}$. Combining (4) and (15), the state-space form of the propeller-pylon-wing aeroelastic equations is formulated as

$$\dot{\boldsymbol{x}} = \begin{bmatrix} \boldsymbol{H}_1\boldsymbol{T}_1\boldsymbol{\Phi}_5 \\ \\ \boldsymbol{H}_5^{-1}\boldsymbol{H}_6 \end{bmatrix}\boldsymbol{x} + \begin{bmatrix} \boldsymbol{H}_2 \\ \\ \boldsymbol{H}_5^{-1}\boldsymbol{H}_7 \end{bmatrix}\dot{\boldsymbol{\alpha}}_{\text{air}} = \boldsymbol{A}_{\text{ss}}\boldsymbol{x} + \boldsymbol{B}_{\text{ss}}\dot{\boldsymbol{\alpha}}_{\text{air}}\,, \tag{17}$$

where $\boldsymbol{\Phi}_5$ is used to select $\boldsymbol{x}_{\text{w}}$ from $\boldsymbol{x}$. Accordingly, the aeroelastic instabilities can be identified by analyzing the eigenvalues of the state matrix $\boldsymbol{A}_{\text{ss}}$. Namely, the propeller-wing system becomes unstable when the real part of one of the eigenvalues becomes positive.

3 NUMERICAL EXAMPLE

The methodology proposed in Section 2 is applied to preliminarily design the wing structure of a DEP aircraft shown in Figure 1(a). This DEP configuration is proposed and developed for a 50 pax regional class hybrid-electric aircraft within the framework of GENESIS project funded by the Clean Sky 2 Joint Undertaking.

In the configuration 1(a), there are five propellers mounted on each side of the wing: One thermal engine (labeled as P1) is placed inboard, and four electric engines (labeled as P2-5) are distributed from semi-span to wing tip. Table 1 lists the main propeller parameters, and note that all four electric engines have an identical design but different mounting positions in both spanwise and chordwise directions.

Table 1: Main propeller parameters of the DEP wing.

Parameter	Thermal engine	Electric engine
Number of blades [-]	4	4
Blade chord [m]	0.259	0.117
Advance ratio [-]	1.269	1.269
Rotor radius [m]	1.965	0.885
Hub radius [m]	0.290	0.130
Rotor mass [kg]	164	85
Motor-nacelle system mass [kg]	831	336

Table 2: Main characteristics of the wing structure.

Wing span	Aspect ratio	Planform area	Root chord	Tip chord	MTOW
24.57 m	11.08	54.50 m^2	2.59 m	1.39 m	23600 kg

The main characteristics of the wing structure is summarized in Table 2. Furthermore, Figure 1(b) illustrates the wing structural analysis model generated by PROTEUS, where the position of propeller concentrated masses and the distribution of fuel and ribs are indicated.

For the definition of wing aeroelastic optimization, Table 3 summarizes the optimization setup. There are in total of $72 \times 8 + 72 = 648$ design variables, because the wing skins and spars are divided into 72 design sections. Regarding to optimization constraints, six laminate feasibility constraints are imposed to each design section, and other constraints listed in Table 3 are given with respect to each load case. In the current work, seven static load cases are considered for wing structural sizing, which are listed in Table 4. Additionally, the composite material properties used for wing sizing are listed in Table 5, and the material of ribs and stringers are chosen to be aluminum alloy.

Table 3: Aeroelastic optimization setup.

Type	Parameter	# variables
Objective	Minimize wing mass	1
Design variables	Lamination parameters	$72 \times 8 = 576$
	Laminate thickness	72
Constraints	Lamination feasibility	$72 \times 6 = 432$
	Static strength	1008 per load case
	Buckling	4608 per load case
	Wing aeroelastic stability	10 per load case
	Aileron effectiveness	1 per load case
	Local angle of attack	34 per load case

In the present 2-DOF propeller model, the frequency and damping coefficient in propeller pitch and yaw motions are required as inputs for propeller structural dynamics [24]. The uncoupled pitch f_θ and yaw f_ψ frequencies are used to calculate pitch $K_\theta = I_\theta(2\pi f_\theta)^2$ and yaw $K_\psi = I_\psi(2\pi f_\psi)^2$ stiffnesses, where I_θ and I_ψ are the propeller mass moments of inertia in pitch and yaw motions, respectively. The pitch g_θ and yaw g_ψ damping coefficients are used to evaluate the structural damping of the nacelle. Although it has been demonstrated that the pitch and yaw stiffnesses have a large influence on propeller whirl flutter [14, 15], it is difficult to obtain these data for a real design of DEP wing. In this work, the pitch and yaw frequencies of each propeller are determined by performing a parametric study, and they are chosen to be the critical pitch

Table 4: Static load cases considered for wing structural sizing.

Load case ID	V_{EAS} (m/s)	Altitude (m)	Mach number	Load factor	Fuel level
1	78.8	0	0.23	2	0.1
2	122.0	0	0.36	2.5	0.9
3	112.5	6090	0.49	1	0.7
4	112.5	6090	0.49	2.5	0.7
5	102.3	0	0.32	-1	0.5
6	111.2	6090	0.48	-1	0.5
7	140.5	6090	0.61	2.5	0.5

Table 5: Composite material properties.

E_{11} (GPa)	E_{22} (GPa)	G_{12} (GPa)	ν_{12}	ρ (kg/m^3)	X_t (MPa)	X_c (MPa)	Y_t (MPa)	Y_c (MPa)	S (MPa)
147.0	10.3	7.0	0.27	1600	948.5	717.6	23.7	94.8	31.6

and yaw frequencies required for providing a stable system of the isolated propeller.

In this work, the aeroelastic stability of a system (either an isolated propeller or a flexible-mount-propeller wing) is assessed using a safety factor defined as $s = V_{\text{ins}}/(1.15V_{\text{D}})$, where V_{ins} is the calculated instability speed of the system and $V_{\text{D}} = 1.25V_{\text{1g}}$ is the aircraft dive speed obtained according to aircraft cruise speed V_{1g}. According to the load cases given in Table 4, V_{ins} has to be higher than 221.4 m/s (true airspeed) to prevent aeroelastic instabilities (i.e., $s \geq 1$).

Figure 3 shows the propeller whirl flutter boundaries obtained by assessing safety factor s with the variation of pitch and yaw frequencies. In Figure 3(a), the whirl flutter boundaries of thermal engine are investigated using different damping coefficients. As it can be expected, increasing nacelle damping enlarges the stable area. For the flutter boundaries of electric engines shown in Figure 3(b), it is clear that the stable region for propeller 2 to 5 are decreased although all four engines are identical. This is because the the distance between propeller mass point and pivot point decreases from propeller 2 to 5, which is indicated by the propeller mass moment of inertia ($I_\theta = I_\psi$) listed in Table 6. Note that, in this work, both the pitch and yaw pivot points are assumed to be located at wing reference axis.

Table 6: Uncoupled pitch and yaw frequencies and damping coefficients chosen for each propeller and the resulted pitch and yaw stiffnesses according to propeller mass moment of inertia.

Propeller ID	P1	P2	P3	P4	P5
Uncoupled frequency [Hz] ($f_\theta = f_\psi$)	4.8	11.7	16.8	26.0	31.4
Damping coefficient [-] ($g_\theta = g_\psi$)	0.005	0.005	0.005	0.005	0.005
Moment of inertia [kg·m^2] ($I_\theta = I_\psi$)	4499	218	127	63	47
Stiffness [kNm/rad] ($K_\theta = K_\psi$)	4092	1178	1415	1681	1829

Table 6 provides the pitch and yaw frequencies and damping ratios chosen for the current study. It is assumed that pitch and yaw motions of the isolated propeller are symmetric, i.e., $f_\theta = f_\psi$ and $g_\theta = g_\psi$. This assumption may lead to a more conservative wing design, because it poses more critical requirements to maintain a stable system compared to the asymmetric pitch and yaw motions. Consequently, the critical uncoupled pitch and yaw frequencies for each propeller can be determined according to the whirl flutter boundaries depicted in Figure 3. Comparing the resulted pitch and yaw stiffnesses, it can be seen that the thermal engine (P1) requires higher

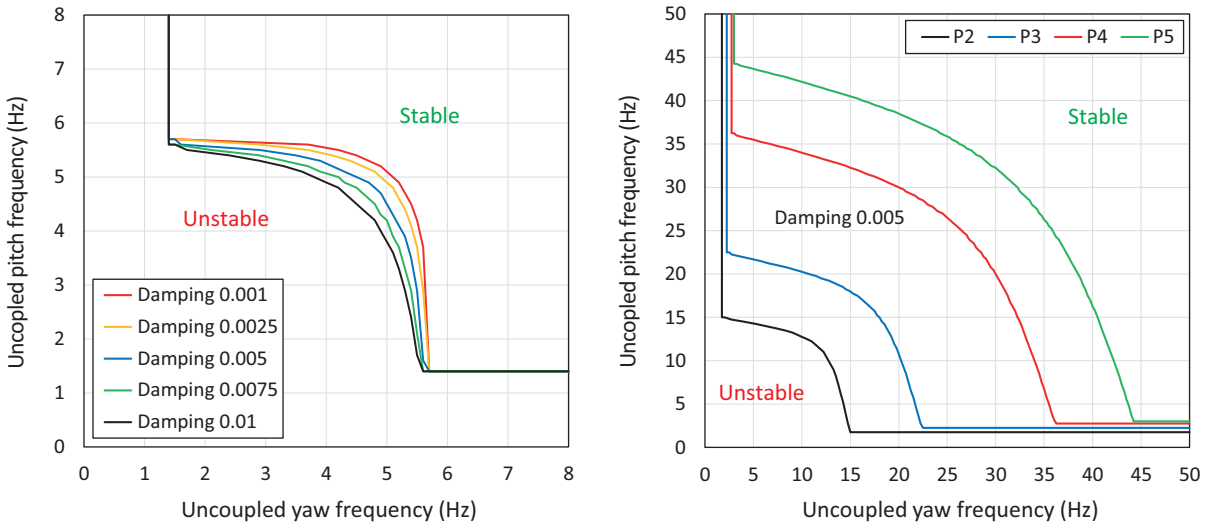

(a) Thermal engine (P1) **(b)** Electric engines (P2-5)

Figure 3: Whirl flutter boundaries of the (a) thermal engine and (b) electric engines.

mounting stiffness than that of electric engines (P2-5) to remain stable. Regarding to electric engines, a stiffer mount is necessary when the propeller is mounted more closer to wing tip.

Figure 4 depicts the result of aeroelastic optimization of wing structures. The objective convergence history is illustrated in Figure 4(a), in which the normalized wing mass reaches a convergent solution after 26 iterations. Figure 4(b) shows the thickness distribution of the optimized wing skins and spars. It can be observed that the wing root region is thicker than other regions to carry aerodynamic loads. Further, as a result of aeroelastic tailoring, some leading edge sections are thicker than their counterparts at trailing edge, which introduces the beneficial wash-out effect to gain the reduction of wing mass.

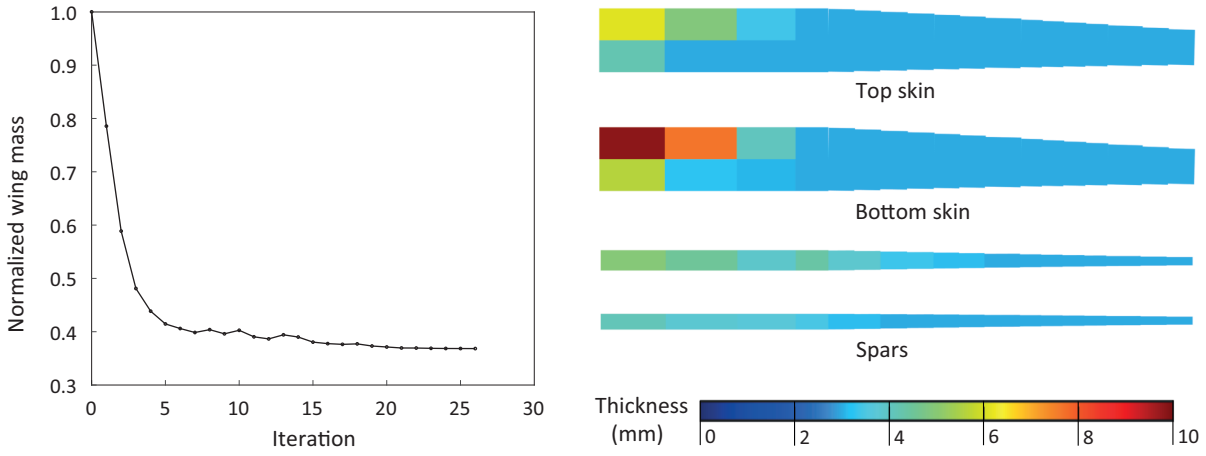

(a) Objective convergence history **(b)** Thickness distribution

Figure 4: Aeroelastic optimization result on (a) objective convergence history and (b) the thickness distribution of the optimized wing skins and spars.

Table 7 lists the natural frequencies of the rigid-mount-propeller wing (obtained from PROTEUS optimization) and the flexible-mount-propeller wing. It indicates that the whirl modes of each propeller are coupled with wing modes, and this coupling has a large dependency on propeller uncoupled pitch and yaw frequencies. For the current DEP configuration, the whirl modes of thermal engine are more crucial than those of electric engines because they are cou-

pled with wing modes at lower frequencies. Further, it can be seen that the pitch frequency of each propeller is decreased due to the coupling between propeller pitch motion and wing torsion, but the yaw frequency remains unchanged because the in-plane motions of the wing has not been considered for propeller-wing coupling in the current work. Additionally, as it can be observed, considering flexible mounts leads to the increase of wing natural frequencies in comparison to the use of rigid mounts.

Table 8 gives the aeroelastic instability type, critical speed and frequency of the rigid-mount-propeller and the flexible-mount-propeller wings. The result indicates that including propeller pitch and yaw DOF into rigid-mount-propeller wing system leads to the decrease of wing flutter speed. Here the instability type for flexible-mount-propeller wing is also referred to as wing flutter, which is because the instability frequency (10.542 Hz) is very close to the 5$^{\text{th}}$ wing natural frequency (10.550 Hz). Further, as shown in the flutter mode shape given in Figure 5, wing deformation is much more pronounced than propeller deflection.

Table 7: Natural frequencies of the rigid-mount-propeller wing (obtained from PROTEUS optimization) and the flexible-mount-propeller wing.

Mode	Rigid mounts [Hz]	Flexible mounts [Hz]
1$^{\text{st}}$ wing mode	1.319	1.376
1$^{\text{st}}$ propeller backward whirl mode	-	4.329
1$^{\text{st}}$ propeller forward whirl mode	-	4.800
2$^{\text{nd}}$ wing mode	2.745	5.398
3$^{\text{rd}}$ wing mode	4.541	7.678
2$^{\text{nd}}$ propeller backward whirl mode	-	10.626
2$^{\text{nd}}$ propeller forward whirl mode	-	11.700
3$^{\text{rd}}$ propeller backward whirl mode	-	15.430
3$^{\text{rd}}$ propeller forward whirl mode	-	16.800
4$^{\text{th}}$ propeller backward whirl mode	-	18.518
4$^{\text{th}}$ propeller forward whirl mode	-	26.000
5$^{\text{th}}$ propeller backward whirl mode	-	26.207
5$^{\text{th}}$ propeller forward whirl mode	-	31.400
4$^{\text{th}}$ wing mode	6.787	34.174
5$^{\text{th}}$ wing mode	10.550	35.362
6$^{\text{th}}$ wing mode	13.914	38.781
7$^{\text{th}}$ wing mode	17.226	43.543
8$^{\text{th}}$ wing mode	23.794	57.187
9$^{\text{th}}$ wing mode	26.789	63.427
10$^{\text{th}}$ wing mode	29.742	70.256

Table 8: Aeroelastic instabilities of the rigid-mount-propeller wing (obtained from PROTEUS optimization) and the flexible-mount-propeller wing.

Instability	Rigid mounts	Flexible mounts
Type	Wing flutter	Wing flutter
Speed V_{ins} [m/s]	376	231
Frequency [Hz]	2.688	10.542
Safety factor s [-]	1.70	1.04

In the present work, the critical mounting stiffness and damping of each propeller (listed in Table 6) are used to assess aeroelastic instability of the current DEP wing. As a consequence,

the safety factor s generally is underestimated, because the propeller mounts in real design are expected to be more stiff. Conversely, the aforementioned flexible-mount-propeller wing system (with safety factor $s = 1.04$) could become unstable if the mounting stiffness and/or structural damping of propellers are lower than their critical values given in Table 6.

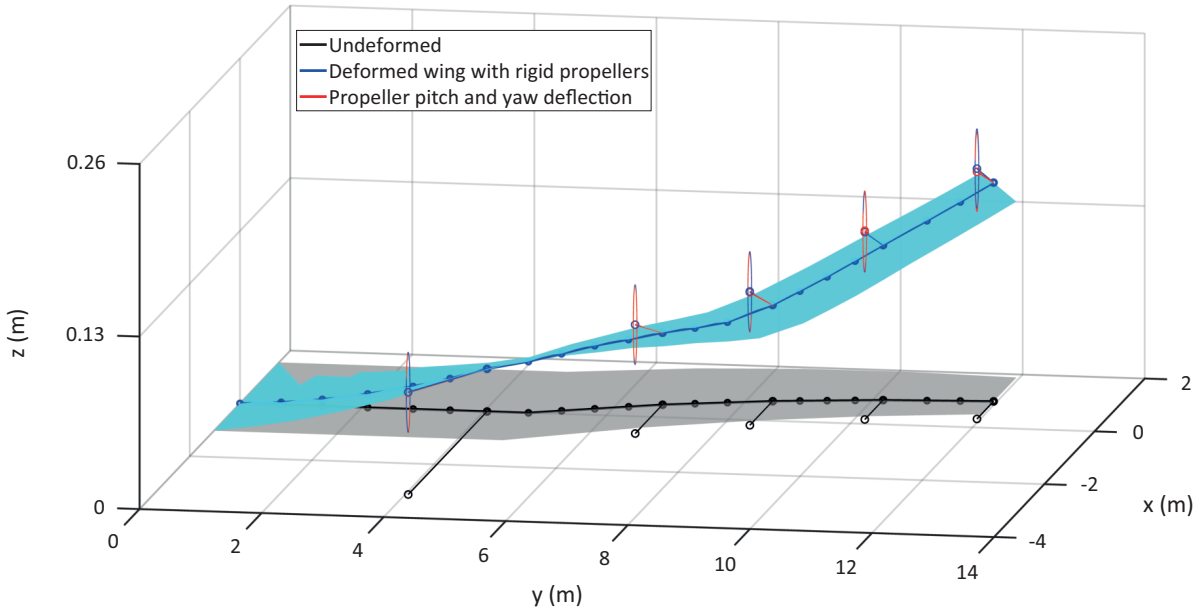

Figure 5: Wing flutter mode shape of the flexible-mount-propeller wing.

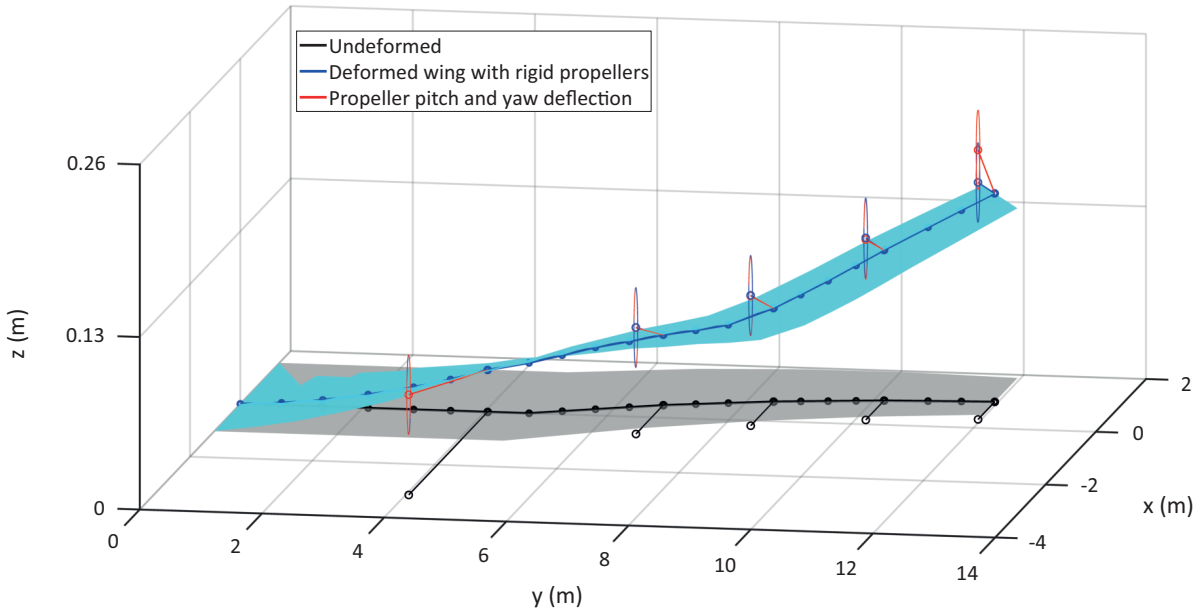

Figure 6: Whirl flutter mode shape of the flexible-mount-propeller wing.

For instance, Figure 6 shows the instability mode shape of the aforementioned propeller-wing system with the predefined input $f_\theta = f_\psi = 4.8$ for all propellers. It can be observed that the deflection of the wing-tip mounted propeller (P5) is more pronounced than that shown in Figure 5 due to the occurrence of propeller whirl flutter. In this specific example, propeller whirl flutter occurs as the result of reducing the mounting stiffnesses of four electric engines. Particularly, the mounting stiffnesses of the wing-tip mounted propeller are reduced more than 90 % compared to their critical mounting stiffnesses given in Table 6, which results in an infeasible DEP design with whirl flutter speed of 39 m/s. This result confirms that the propeller mounting

properties have a large impact on aeroelastic instabilities of the DEP wing system.

4 CONCLUSIONS

To enable the consideration of propeller whirl flutter for the preliminary design of DEP aircraft wings, this work extends an existing in-house tool, PROTEUS, by including a post-processing procedure on whirl flutter analysis. In the extended framework, the composite wing structures can be optimized for minimal wing mass, subject to the design constraints on wing aeroelastic stability, aileron effectiveness, material strength and buckling load. In the optimization process, the distributed propellers are modeled as concentrated masses, so that their effect on wing sizing can be considered by including the mass inertia into the global mass matrix in wing structural model. In order to assess the aeroelastic instability of the optimized DEP wing, an aeroelastic model of fully coupled propeller-wing system is built within the framework of PROTEUS. In this model, pitch and yaw motions are considered to describe propeller DOF, and they are coupled with the heave and torsional motions of wing structural beam model. Further, the aerodynamic effect of propellers on wing characteristics is taken into account by adding propeller aerodynamic loads on wing structural model. Finally, the aeroelastic model is formulated into a state-space form, so that the instabilities of the coupled propeller-wing system can be identified by analyzing the eigenvalues of the state matrix.

To demonstrate the usefulness of the proposed method, it has been applied to design the wing structure of a DEP configuration developed in GENESIS project. Moreover, a parametric study has been carried out to determine the inputs for calculating propeller mounting properties. The result indicates that including propeller pitch and yaw DOF into rigid-mount-propeller wing system leads to the decrease of wing flutter speed. Further, it has been also confirmed that the propeller mounting properties have a large influence on aeroelastic instability of the coupled propeller-wing system. In the proposed method, the propeller whirl flutter is assessed in a post-processing procedure regarding to an optimized wing, which excludes the effect of whirl flutter on wing structural sizing. This limitation will be addressed in future work by means of including whirl flutter speed as a design constraint in aeroelastic optimization. In addition, by making use of the proposed framework, the effects of wing geometry (e.g., chord length) and propeller mounting position on aeroelastic instability of a DEP wing can be investigated, which is also considered as a future work.

5 ACKNOWLEDGEMENTS

This study is part of the GENESIS project, which has received funding from the Clean Sky 2 Joint Undertaking (JU) under grant agreement No 101007968. The JU receives support from the European Union's Horizon 2020 research and innovation programme and the Clean Sky 2 JU members other than the Union. This work only reflects the authors' views; the JU is not responsible for any use that may be made of the information it contains.

6 REFERENCES

[1] Brelje, B. J. and Martins, J. R. R. A. (2019). Electric, hybrid, and turboelectric fixed-wing aircraft: A review of concepts, models, and design approaches. *Progress in Aerospace Sciences*, 104, 1–19.

[2] Moore, J. B. and Cutright, S. (2017). Structural design exploration of an electric powered multi-propulsor wing configuration. In *58th AIAA/ASCE/AHS/ASC Structures, Structural Dynamics, and Materials Conference*. p. 0203.

[3] Hoover, C. B., Shen, J., and Kreshock, A. R. (2018). Propeller whirl flutter stability and its influence on X-57 aircraft design. *Journal of Aircraft*, 55(5), 2169–2175.

[4] Afonso, F., Vale, J., Oliveira, É., et al. (2017). A review on non-linear aeroelasticity of high aspect-ratio wings. *Progress in Aerospace Sciences*, 89, 40–57.

[5] Amoozgar, M., Friswell, M. I., Fazelzadeh, S. A., et al. (2021). Aeroelastic stability analysis of electric aircraft wings with distributed electric propulsors. *Aerospace*, 8(4), 100.

[6] Deere, K. A., Viken, J. K., Viken, S. A., et al. (2017). Computational analysis of a wing designed for the X-57 distributed electric propulsion aircraft. In *35th AIAA Applied Aerodynamics Conference*. p. 3923.

[7] Hoover, C. B. and Shen, J. (2018). Parametric study of propeller whirl flutter stability with full-span model of X-57 Maxwell aircraft. *Journal of Aircraft*, 55(6), 2530–2537.

[8] Heeg, J., Stanford, B. K., Kreshock, A., et al. (2019). Whirl flutter and the development of the NASA X-57 Maxwell. In *International Forum on Aeroelasticity and Structural Dynamics*, NF1676L-31615.

[9] Johnson, W. (1994). Technology drivers in the development of CAMRAD II. In *American Helicopter Society Aeromechanics Specialists Conference, San Francisco, California*.

[10] Bauchau, O. A., Bottasso, C. L., and Nikishkov, Y. G. (2001). Modeling rotorcraft dynamics with finite element multibody procedures. *Mathematical and Computer Modelling*, 33(10-11), 1113–1137.

[11] Kunz, D. L. (2005). Analysis of proprotor whirl flutter: Review and update. *Journal of Aircraft*, 42(1), 172–178.

[12] Cecrdle, J. (2015). *Whirl flutter of turboprop aircraft structures*. Woodhead Publishing.

[13] Yeo, H. and Kreshock, A. R. (2020). Whirl flutter investigation of hingeless proprotors. *Journal of Aircraft*, 57(4), 586–596.

[14] Böhnisch, N., Braun, C., Koschel, S., et al. (2022). Whirl flutter for distributed propulsion systems on a flexible wing. In *AIAA SCITECH 2022 Forum*. p. 1755.

[15] Koch, C. (2021). Parametric whirl flutter study using different modelling approaches. *CEAS Aeronautical Journal*, 1–11.

[16] Werter, N. P. M. and De Breuker, R. (2016). A novel dynamic aeroelastic framework for aeroelastic tailoring and structural optimisation. *Composite Structures*, 158, 369–386.

[17] IJsselmuiden, S. T., Abdalla, M. M., and Gürdal, Z. (2008). Implementation of strength-based failure criteria in the lamination parameter design space. *AIAA Journal*, 46(7), 1826–1834.

[18] Khani, A., IJsselmuiden, S. T., Abdalla, M. M., et al. (2011). Design of variable stiffness panels for maximum strength using lamination parameters. *Composites Part B: Engineering*, 42(3), 546–552.

[19] Dillinger, J. K. S., Klimmek, T., Abdalla, M. M., et al. (2013). Stiffness optimization of composite wings with aeroelastic constraints. *Journal of Aircraft*, 50(4), 1159–1168.

[20] Hammer, V. B., Bendsøe, M. P., Lipton, R., et al. (1997). Parametrization in laminate design for optimal compliance. *International Journal of Solids and Structures*, 34(4), 415–434.

[21] Raju, G., Wu, Z., and Weaver, P. M. (2014). On further developments of feasible region of lamination parameters for symmetric composite laminates. In *55th AIAA/ASMe/ASCE/AHS/SC Structures, Structural Dynamics, and Materials Conference*. p. 1374.

[22] Wu, Z., Raju, G., and Weaver, P. M. (2015). Framework for the buckling optimization of variable-angle tow composite plates. *AIAA Journal*, 53(12), 3788–3804.

[23] Wang, Z., Peeters, D., and De Breuker, R. (2021). Aeroelastic optimisation of manufacturable tow-steered composite wings with cruise shape constraint and gust loads. In *IOP Conference Series: Materials Science and Engineering*, vol. 1024. IOP Publishing, p. 012020.

[24] Liu Xu, V. Q. (2020). *Propeller-wing whirl flutter: An analytical approach*. Delft University of Technology.

[25] Houbolt, J. C. and Reed, W. H. (1962). Propeller-nacelle whirl flutter. *Journal of the Aerospace Sciences*, 29(3), 333–346.

COPYRIGHT STATEMENT